Extension-Enhanced Conductivity of Liquid Crystalline Polymer Nano-Composites

Hong Zhou,[1] *M. Gregory Forest,**[2] *Xiaoyu Zheng,*[2] *Qi Wang,*[3] *Robert Lipton*[4]

[1] Department of Applied Mathematics, Naval Postgraduate School, Monterey, CA 93943-5121, USA
[2] Program in Applied Mathematics, Institute for Advanced Materials, Nanoscience & Technology, University of North Carolina, Chapel Hill, NC 27599-3250, USA
E-mail: forest@amath.unc.edu
[3] Department of Mathematics, Florida State University, Tallahassee, FL 32306-4510, USA
[4] Department of Mathematics, Louisiana State University, Baton Rouge, LA 70803-4918, USA

Summary: Our aim here is to predict elongational flow-induced enhancements in thermal or electrical conductivity of liquid crystal polymer (LCP) nano-composites. To do so, we combine two classical mathematical asymptotic analyses: slender longwave hydro-thermo-dynamics for fibers and exact analysis of pure elongation of LCPs in solvents for bulk phases without boundary effects; and homogenization theory for effective properties of low volume-fraction spheroidal inclusions. Two implications follow: elongational flow dominates fiber free surface and thermal effects on electrical and thermal conductivity enhancements; and, there appears to be no sacrifice in enhancements by producing much higher radius, bulk fibers.

Keywords: conductivity; fibers; homogenization; liquid crystal polymers; nano-composites

Introduction

Ultra-strength textile fibers, e.g. Vectran and Kevlar, achieve distinguished properties as a result of interactions between macroscopic elongation-dominated hydrodynamics, microscopic orientation dynamics of liquid crystalline polymer (LCP) molecules, free surface drag effects, and thermodynamics. Recently direct spinning of carbon natotube fibers from chemical vapor deposition synthesis is made possible which will provide many potential applications.[1]

In the manufacturing of LCP fibers, the melt or solution is extruded through a spinneret into cross-flowing air. The fiber is pulled downstream, past the solidification transition, at a speed considerably above the extrusion speed, effecting large extension rates along the filament. Process simulations provide a useful tool for exploring the effect of changes in

 DOI: 10.1002/masy.200551007

operating variables (extrusion temperature, air velocity, take-up speed, etc.) and material properties (molecular as well as LCP melt or solution rheology) on the properties of the spun filament. Isothermal spinning flows of liquid crystalline polymers have been studied[2, 3, 4] and extended to thermotropic liquid crystalline polymer (TLCP) spin processes.[5, 6]

The first goal of this article is to apply our TLCP spin model to predict electrical or thermal conductivity properties of spun fibers. Second, we compare fiber conductivity enhancements with pure elongation flow-induced conductivity, which is a consequence of flow and molecular orientation dynamics uncoupled from thermal and surface drag effects. The article is organized as follows. First we briefly recall the asymptotic 1-D TLCP model. We then introduce the effective conductivity tensor of low volume fraction composites from Zheng et al.[7] Finally, we present numerical results on conductivity in thermal and isothermal fiber spinning and isothermal pure elongational flow. We give results for rod-like LCPs, although the same methods apply to discotic molecules.

Asymptotic 1-D TLCP Fiber Spinning Model

The full 3-D model is based on a Doi-type mesoscopic theory for nematodynamics, along with empirical correlations and rheological relations that are consistent with the solution processing of TLCPs.[5, 6] Exploiting the fact that the fiber is very thin with a typical aspect ratio of the order 10^{-4}, we have derived the 1-D nonisothermal slender model for axisymmetric TLCP filaments.[5, 6] Let ϕ be the free surface radius, v the axial velocity, s the uniaxial order parameter, and T the temperature. The leading order equations are:

$$\left(\phi^2\right)_t + \left(v\phi^2\right)_z = 0$$

$$\left(\phi^2 v\right)_t + \left(\phi^2 v^2\right)_z = \frac{1}{F}\phi^2 + \frac{1}{W}\phi_z + \left[\phi^2\left(R_{eff}^{-1}(s,T)\,v_z + \alpha TU(s)\right)\right]_z - \beta v^{\gamma}\phi^{\gamma-1} \tag{1}$$

$$s_t + vs_z = v_z(1-s)(2s+1) - \sigma_d \Lambda^{-1}(T)\,U(s)$$

$$T_t + vT_z = \frac{1}{Pe}\phi^{-2}\left(\phi^2 T_z\right)_z - 2St\phi^{-1}\left[(v\phi)^m \phi^{-1}\right](T - T_a) + \frac{Br}{Pe}\left[R_{eff}^{-1}(s,T)\,v_z + \alpha TU(s)\right]v_z,$$

where the Froude number F and the Weber number W, respectively characterize gravity and surface tension relative to inertia; the Peclet number Pe and the Brinkman number Br, respectively parametrize specific heat and viscous heating relative to thermal conductivity; the Stanton number St measures the dimensionless heat transfer coefficient; the parameters α, β and σ_d respectively describe the molecular kinetic energy per unit volume relative to

inertial energy per unit volume, dimensionless drag coefficient and anisotropic drag parameter; Λ(T) is the scaled LCP relaxation time,

$$\Lambda(s,T) = \Lambda_0 e^{\omega\left(\frac{1}{T}-1\right)},$$

where Λ_0 and ω are determined by rheology data at a fixed temperature. R_{eff} (s,T) is an effective 1-D flow-orientation Reynolds number,

$$R_{eff}^{-1}(s,T) = \frac{3}{\mathrm{Re}} e^{\varepsilon\left(\frac{1}{T}-1\right)} + 2\alpha T\Lambda(T)\dot{s}^2,$$

consisting of an isotropic Newtonian and an elastic orientation-dependent contribution; the integral of U(s) defines the uniaxial bulk free energy, whose critical points versus dimensionless LCP concentration N give the isotropic-nematic phase diagram,

$$U(s) = s\left[1 - \frac{N}{3}(1-s)(2s+1)\right]. \tag{2}$$

The other two leading order unknowns are u, the radial velocity, and p, the pressure, which are prescribed by

$$u = -\frac{v_z}{2}$$

$$p = -\frac{1}{W}\phi^{-1} - \frac{1}{\mathrm{Re}} e^{\varepsilon\left(\frac{1}{T}-1\right)} v_z - \frac{1}{3}\alpha T U(s) + \frac{2}{3}\alpha\Lambda(T)T(1-s)sv_z.$$

For steady state solutions the equation of continuity (1)a integrates to

$$\phi^2 v = 1,$$

and the computational domain is scaled to $0 \le z \le 1$. The upstream location $z = 0$ is chosen past the spinneret, beyond the swell region so that the longwave asymptotic approximation is satisfied. To be consistent with the nondimensionalization, fixed upstream boundary conditions are placed on fiber radius, velocity, and temperature:

$$\phi(0) = 1,\ v(0) = 1,\ T(0) = 1.$$

The downstream thermal boundary condition is selected by assuming that axial thermal conduction is negligible,

$$\left.\frac{\partial\left(\phi^2 T_z\right)}{\partial z}\right|_{z=1} = 0.$$

The other two boundary conditions, s(0) and the draw ratio v(1), are free processing parameters which need to be specified in the simulations. The upstream degree of

orientation, s(0), is a function of spinneret design, whereas the take-up speed v(1) (the so-called draw ratio) measures process speed and throughput.

Effective Conductivity Tensors

Recently Zheng et al.[7] applied homogenization theory to predict the effective conductivity tensor, σ^e, for uniform suspensions of spheroidal nano-inclusions with conductivity σ_2 and volume fraction θ_2 in a matrix of conductivity σ_1. Conductivity obeys elliptic equations which are virtually identical for thermal, electric, and dielectric properties. Here we focus on the effective thermal conductivity, σ^e, of LCPs in a solvent whose ratio of conductivities is highly contrasted, $\sigma_2/\sigma_1 >> 1$ or $\sigma_1/\sigma_2 << 1$. The nano-elements are from high aspect ratio (length-to-diameter ratio) nematic liquid crystalline polymers, either rod-like or platelet spheroids. Using the fact that the overall conductivity properties of polymer nano-composites are well approximated by the effective conductivity tensor in the low volume fraction regime of the included phase and the effective conductivity is in turn strongly influenced by the orientation distribution of the nano-inclusions and exploiting the results of Doi-Hess kinetic theory of the orientational probability distribution at both isotropic and order volume fractions, they have derived the effective conductivity tensor in close form:

$$\sigma^{\mathbf{e}} = \sigma_1\mathbf{I} + \sigma_1\theta_2(\sigma_2-\sigma_1)\left\{\frac{2}{\sigma_2+\sigma_1-(\sigma_2-\sigma_1)L_a}\mathbf{I} + \frac{(\sigma_2-\sigma_1)(1-3L_a)}{\left[(\sigma_2+\sigma_1)-(\sigma_2-\sigma_1)L_a\right]\left[\sigma_1+(\sigma_2-\sigma_1)L_a\right]}\mathbf{M}(f)\right\} + O(\theta_2^2),$$

where $\mathbf{I}$ is the 3 by 3 identity matrix, L_a is the spheroidal depolarization factor depending on the aspect ratio r of the molecular spheroids through the relation

$$L_a = \frac{1-\varepsilon^2}{\varepsilon^2}\left[\frac{1}{2\varepsilon}\ln\left(\frac{1+\varepsilon}{1-\varepsilon}\right)-1\right], \quad \varepsilon = \sqrt{1-r^{-2}}.$$

f is the orientational probability distribution function of the LCP inclusions, governed by the Smoluchowski equation of the Doi-Hess kinetic theory for quiescent or flowing nematic polymers; $\mathbf{M}(f)$ is the second-moment of the orientation probability density f, which is the object of mesoscopic closure models from which the thin fiber equations were derived. [2, 3, 4, 5, 6] For uniaxial orientation distributions, in which the orientation transverse to the fiber axis is isotropic, $\mathbf{M}(f)$ is related to the order parameter s by

$$\mathbf{M}(f) = s\left(\mathbf{nn} - \frac{\mathbf{I}}{3}\right) + \frac{\mathbf{I}}{3}$$

where **n** is the principal orientation axis, which converges downstream to the fiber axis of symmetry. Upstream, the LCP solution is generally in a biaxial phase, where **M**(*f*) is prescribed by two order parameters, s and β,

$$\mathbf{M}(f) = s\left(\mathbf{n}_1\mathbf{n}_1 - \frac{\mathbf{I}}{3}\right) + \beta\left(\mathbf{n}_2\mathbf{n}_2 - \frac{\mathbf{I}}{3}\right) + \frac{\mathbf{I}}{3},$$

where $\mathbf{n}_1$ and $\mathbf{n}_2$ are two major directors, or principal axes, of the orientation distribution. One can explicitly calculate the distinct principal values (eigenvalues) σ_j^e and corresponding principal axes $\mathbf{n}_j$ of the conductivity tensor σ^e, and then determine relative conductivity *enhancements* $\mathcal{E}_j$:

$$\mathcal{E}_j = \frac{\sigma_j^e - \sigma_1}{\sigma_1}, \quad j = 1,2,3.$$

The maximum conductivity enhancement $\varepsilon_{max}=\max(\varepsilon_j)$, which for fiber spinning flows is associated with conductivity along the spun fiber axis, and for pure extensional flows is described below. Anisotropy in conductivity is measured by $\max(\varepsilon_{max} - \varepsilon_j)$, which indicates the contrast in conductivity along and transverse to the principal axes of σ^e.

Effective Conductivity Enhancement in Both Fiber Spinning Flow and Pure Elongation Flow

In order to see how effective conductivity is enhanced in fiber spinning flow, we first solve the steady state solutions of (1), confirm their stability by both time-dependent simulations and stability analysis,[5, 6] and then compute the maximum conductivity enhancement. Figure 1 shows both the maximum anisotropy in conductivity (top panel) and the maximum conductivity enhancement (bottom panel) as a function of the spun fiber radius for both isothermal and thermal cases. In this study we use polymer-CNT (carbon nanotube) composites as a model example, where the polymer matrix typically has an intrinsically low thermal conductivity on the order of 0.15 to 0.30 W/m K and the CNTs are metallic. The CNTs exhibit a high aspect ratio, with the length generally several μm and the diameter approximately 0.4 to 100 nm. In all the calculations presented in this paper the aspect ratio r = 1000, the thermal conductivity of the nanotubes is taken as 2000 W/m K and that of polymeric materials as 0.20 W/m K. [8, 9] As a result, $\sigma_1/\sigma_2=10^{-5}$.

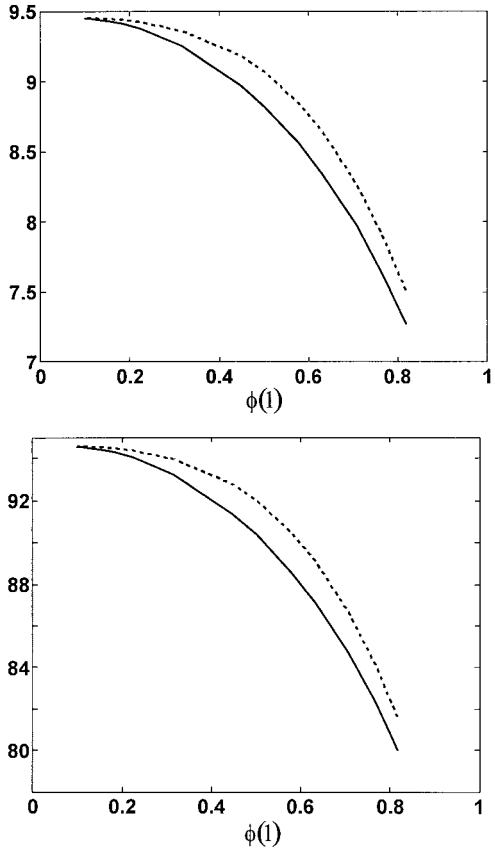

Figure 1. The maximum anisotropy in conductivity (top panel) and the maximum conductivity enhancement (bottom panel) as a function of the spun fiber radius $\phi(1)$ for both isothermal (solid line) and thermal (dashed line) cases.

In figure 2 we depict the maximum effective conductivity enhancement as a function of the volume fraction θ_2 which is related to the aspect ratio r and the dimensionless concentration parameter N by

$$\theta_2 = \frac{\pi}{8r} N.$$

As shown here, the maximum effective conductivity enhancement behaves as a monotone increasing function of the volume fraction.

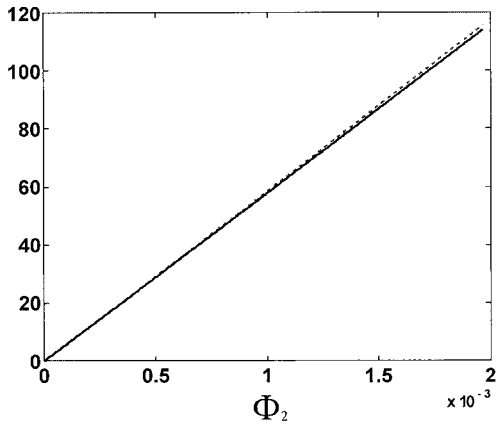

Figure 2. The maximum effective conductivity enhancement as a function of the volume fraction θ_2.

For comparison purposes, next we consider *pure elongation-induced monodomains* at isotropic and nematic concentrations. These predictions address the influence of an imposed linear extensional flow on molecular orientation, which is a poor man's approximation to fiber extensional flow, while suppressing the effects of free surfaces, temperature, and boundary conditions. The dimensionless flow field for pure elongation, in rectangular coordinates (x,y,z) with respect to the basis $(\mathbf{e}_x,\mathbf{e}_y,\mathbf{e}_z)$, is $\mathbf{v} = Pe\left(-\frac{x}{2},-\frac{y}{2},z\right)$.

Here *Pe* is Peclet number, the critical flow/orientation dimensionless parameter, describing the ratio of the elongational rate and the orientational relaxation rate (Λ_0 above). For $Pe > 0$, the flow stretches along the *z* axis, called axial or unidirectional elongation; for $Pe < 0$, the flow stretches radially in the entire *xy*-plane, called planar or bidirectional elongation. The governing biaxial order parameter equations in imposed elongational flows are [6, 10]

$$s_t = Pe\left(1-\beta+s+\beta s-2s^2\right)-U(s)+\frac{2}{3}Ns\beta(s-\beta-1)$$

$$\beta_t = Pe\left(\beta^2-2\beta s-\beta\right)-U(\beta)+\frac{2}{3}Ns\beta(\beta-s-1),$$

where U(s) is defined in (2). We have determined the full set of stable (and unstable) elongation-induced equilibria.[6, 10, 11] From these earlier results, the stable elongation-induced equilibria and their corresponding maximum effective conductivity enhancement versus volume fraction, for both axial and planar elongation, is illustrated in Figure 3 (where $Pe \geq 0$) and Figure 4 (where $Pe \leq 0$). We give results for rod-like LCP molecules

here. $Pe = 0$ corresponds to the quiescent case, where isotropic and nematic equilibria co-exist in a narrow window of bi-stability. We display $Pe \neq 0$ which have already "pulled out'' the bi-stable phases, and unique stable phases remain.

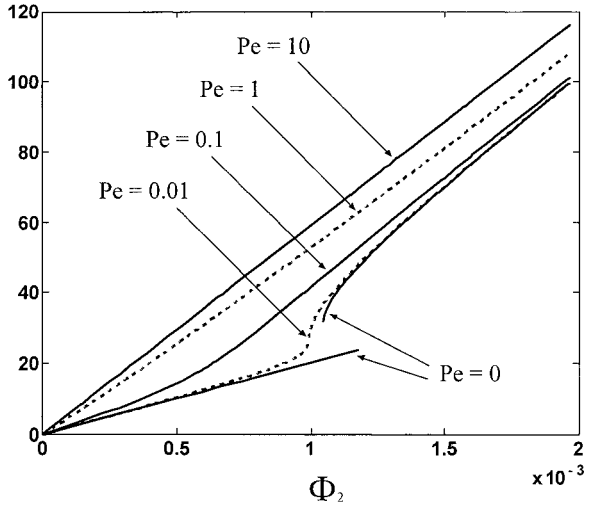

Figure 3. Elongation-induced maximum effective conductivity enhancement versus volume fraction for axial elongation.

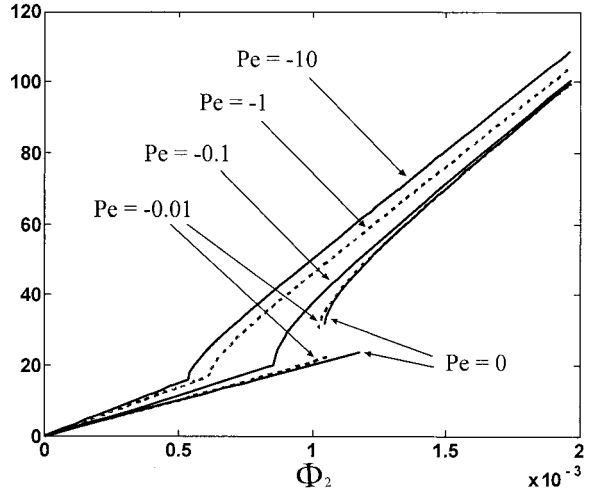

Figure 4. Elongation-induced maximum effective conductivity enhancement versus volume fraction for planar elongation.

From Figure 2 and Figure 4 it is clear that when the elongation rate is high enough, the maximum effective conductivity enhancement behaves almost the same for both the fiber spinning flow and the pure axial elongation flow.

Conclusions

These results predict that surface and thermal effects are negligible at sufficiently high extension rates relative to the effects of nematic orientation and elongation enhancements on thermal and electrical composite properties. Perhaps the practical limitation here is the elongational viscosity of the liquid nano-composite, putting limits on extension rates. For volume-averaged properties, ignoring percolation behavior, these results imply there is no thermal or electrical property compromise in producing much larger fibers, rather than traditional thin fibers which must be bundled together.

Acknowledgements

Effort sponsored by the Air Force Office of Scientific Research, Air Force Materials Command, USAF, under grant no. F49620-02-1-0086, the National Science Foundation through grants DMI-0115445, DMS-0204243 and DMS-0308019, and the Army Research Office through grant 47089-MS-SR. This work is supported in part by NASA University research, Engineering and Technology Institute on Bio-Inspired Materials (BIMat) under award no. NCC-1-02037.

[1] Y. Li, I. A. Kinloch, A. H. Windle, *Science*, **2004,** 276.
[2] S. Ramalingam, R. C. Armstrong, *J. Rheol.*,**1993**, ***37,*** 1141.
[3] M. G. Forest, Q. Wang, S. E. Bechtel, *Physica D*, **1997,** *99,* 527.
[4] M. G. Forest, Q. Wang, S. E. Bechtel, *J. Rheol.,* **1997,** *41,* 821
[5] M. G. Forest, H. Zhou, Q. Wang, *Advances in Polymer Technology*, **1999,** ***18***, 314.
[6] M. G. Forest, H. Zhou, Q. Wang, *SIAM J. Appl. Math.*, **2000**, 60, 1177.
[7] X. Zheng, M. G. Forest, R. Lipton, R. Zhou, Q. Wang, *Advanced Functional Materials*, **2004**, in press.
[8] S. U. S. Choi, Z. G. Zhang, W. Yu, F. E. Lockwood, E. A. Gruike, *Appl. Phys. Lett.*, **2001**, *79*, 2252.
[9] C. Liu, P. T. Mather, *ANTEC*, **2004**, 3080.
[10] M. G. Forest, Q. Wang, H. Zhou, *Phys. Fluids*, **2000**, *12*, 490.
[11] M. G. Forest, Q. Wang, H. Zhou, *Liquid Crystals*, **2001**, 28, 717
[12] R. A. Vaia, ``*Polymer Nanocomposites*'', Oxford University Press 2002.